Experimental Investigation on the Turbulence Augmentation of a Gun-type Gas Burner by Slits and Swirl Vanes

Jang-kweon Kim*
Power Mechanical System Engineering Major Kunsan National University
573-701 San 68, Miryong-Dong, Kunsan, Chonbuk, Korea

The purpose of this paper is to investigate the effects of slits and swirl vanes on the turbulence augmentation in the flow fields of a gun-type gas burner using an X-type hot-wire probe. The gun-type gas burner adopted in this study is composed of eight slits and swirl vanes located on the surface of an inclined baffle plate. Experiment was carried out at a flow rate of 450 *l*/min in burner model installed in the test section of subsonic wind tunnel. Swirl vanes play a role diffusing main flow more remarkably toward the radial direction than axial one, but slits show a reverse feature. Consequently, both slits and swirl vanes remarkably increase turbulence intensity in the whole range of a gun-type gas burner with a cone-type baffle plate.

Key Words : Gun-Type Gas Burner, Hot-Wire Anemometer, Slit, Subsonic Wind Tunnel, Swirl Flow, Swirl Vane, Turbulence Augmentation, X-probe

1. Introduction

Usually, most gas combustors adopt various kinds of burners that accompany swirl flow. Swirl flow has been widely investigated for several decades because it provides flame stabilization, short flame, high combustion intensity, and enhanced mixing between fuel and air. Therefore, the swirl flow is usually used extensively in gas turbine, boiler, industrial furnace, ram jet, and jet mixer, etc (Beer et al., 1972 ; Froud et al., 1995 ; Lefebvre, 1983 ; Shioji et al., 1998 ; Syred et al., 1974 ; Tsao et al., 1999).

The combustion characteristics of a gas burner are influenced by various factors such as ingredient of fuel gas, diffusion of injected gas, flow characteristics, and mixing between fuel gas and air, etc. Because the mixing rate between fuel gas and air was the most important variable among them for perfect combustion state, the swirl flow has been coming up as an effective means (Hibara et al., 1999).

Many experiments on swirl flows that are commonly used in a gas burner have been carried out from simple single swirl burners to very complex actual gas swirl combustors. These studies have examined closely the general characteristics of swirl flows and revealed the important effects of swirl flow on promoting flame stability, increasing combustion efficiency, and controlling the emission of combustion pollutants (Gupta et al., 1984).

Beer et al. (1972) and Lefebvre (1983) mentioned that recirculation zone and high turbulence level are formed under the adverse pressure gradient along the axial distance with introducing a strong swirl in the ambient air flow of a concentric jet burner. Syred et al. (1974) showed that strongly swirling jets in a swirl burner cause a large recirculation region around the jet exit by vortex breakdown phenomenon corresponding to the rapid axial deceleration of the swirling flow. In addition, they also revealed that the large recirculation region promotes the entrainment rate of surrounding fluid, fast mixing between fuel

* **E-mail** : flowkim@kunsan.ac.kr
TEL : +82-63-469-1848; **FAX** : +82-63-469-1841
Power Mechanical System Engineering Major Kunsan National University 573-701 San 68, Miryong-Dong, Kunsan, Chonbuk, Korea (Manuscript **Received** November 22, 2003; **Revised** June 21, 2004)

and air, and flame stabilization by shortening flame length. Leuckel et al. (1976) conducted various measurements of a non-premixed single concentric swirl burner under the condition of putting an annular pipe to swirling air jet and a central one to nonswirling fuel jet, respectively. Chen et al. (1988) examined the enhanced mixing characteristics in swirl flows through the formation of a central toroidal recirculation zone. Gupta et al. (1976) obtained fairly different flame stability limits, turbulence levels, volumetric heat release rates, and combustion characteristics by controlling the axial and angular momentum of the jets in the double concentric burner.

In this study, the gun-type gas burner with a cone-type baffle plate was selected for the purpose of applying to a gas furnace having a heating capacity of 15,000kcal/hr. On the other hand, the turbulent flow fields for this gas burner have been investigated to various ways by author (Kim, 2001a; 2001b; 2001c; 2003; Kim et al., 2003; 2004). However, because the gas burner consists of eight swirl vanes and slits situated on the front of a circular draft tube geometrically, it is necessary to grasp how much slits and swirl vanes contribute to turbulence augmentation in the main flow of a gas burner. For this purpose, three kinds of burner shape models were considered in this study; for example, a main gas burner, a burner model with only slits, and a burner one with only swirl vanes. Therefore, the mean velocity and the turbulence intensity, etc. were measured with a hot-wire anemometer system without combustion chamber in order to compare and analyze the results obtained from three burner models.

2. Experimental Apparatus and Method

2.1 Experimental apparatus

Figure 1 represents the details of a gun-type gas burner tested in this experiment. This gas burner has a cone-type baffle plate inclined about 45-degree to the front of a circular draft tube. This cone-type baffle plate is composed of eight swirl vanes located in the inclined baffle plate and eight

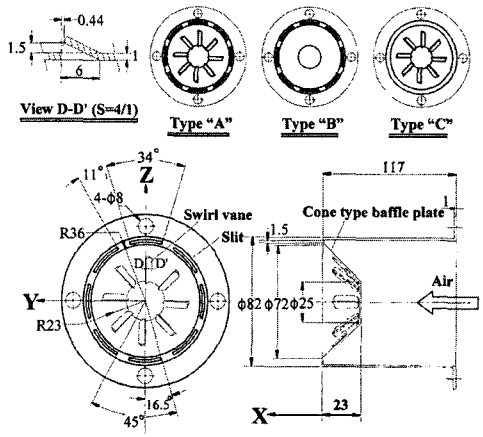

Fig. 1 Configuration of a gas burner model

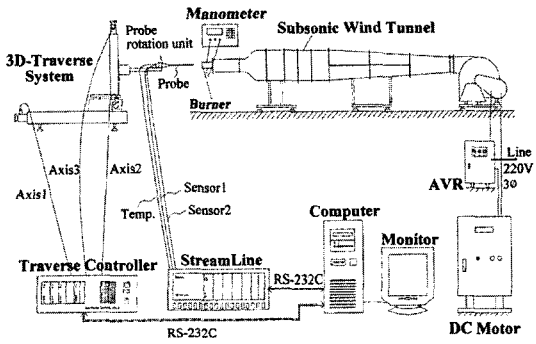

Fig. 2 Schematic diagram including hot-wire anemometer system

narrow slits located just above a swirl vane as well as situated radially on the edge of a gas burner. Here, the alphabets of X, Y, and Z mean an axial distance, a horizontal radial one, and a vertical radial one, respectively.

Figure 2 shows an experimental apparatus for measuring flow velocities using a hot-wire anemometer system. Here, the burner models were installed in the exit of the test section of a subsonic wind tunnel.

The subsonic wind tunnel consists of a centrifugal fan and DC motor having a capacity of 3.75kW (220V, 3 Phase), a diffuser, a tranquilization chamber, a contraction, and a test section. Moreover, its maximum velocity is 35m/s in the test section of 220mm (width) x 220mm (height) x 410mm (length) in size. The turbulence intensity in the central part of the test section is less than about 0.4% at the mean flow velocity of

about 13m/s.

On the other hand, a hot-wire anemometer system (Dantec 90N10 Streamline) used for measuring turbulent flow in the state of non-combustion is composed of a constant temperature type hot-wire anemometer, a calibrator capable of doing velocity and directional calibration at the same time (Dantec 90H01 & 90H02), a three-dimensional automatic traversing system (Dantec 41T50 & 41T75), and a personal computer (PC). It was controlled by a PC through RS-232C interface, and the calibrator is connected with an air compressor capable of operating up to the extent of the effective pressure of 10kg/cm^2.

2.2 Experimental method

In this study, an X-type hot-wire probe (Dantec, 55R51) was used for measuring flow velocity. The calibrated velocities and the mean yaw factors required for an X-probe were obtained by the calibration procedure of the flow velocity and the flow direction, respectively.

The velocity calibration was carried out from zero to 20m/s. Here, the accuracy of velocity was obtained below about 0.4% through the fifth order polynomial curve fit analysis. Also, the directional sensitivity of the X-probe was checked by changing the yaw angle from −40° to +40° at 10-degree intervals for a constant flow velocity of 10m/s. In consequence of the directional calibration procedure, the mean yaw factors per channel, used to calculate the calibrated velocity from raw signal data for hot-wires, were obtained as 0.064 and 0.074 in the case of Type A as well as 0.088 and 0.106 in the case of Type B and Type C (Kim, 2001 ; 2003 ; Kim et al., 2003).

The sampling rate and the number of total sampling data per channel are 20kHz and 102, 400, respectively. Also, the low-pass filter was set up with 30kHz per channel. Moreover, the exit velocity of a burner model was controlled under the static pressure of 164 Pa collected from the four pressure taps attached on the surface of the circular draft tube of a burner model. Here, the static pressure corresponds to the flow rate of 450 *l*/min utilized for actual combustion air flow rate.

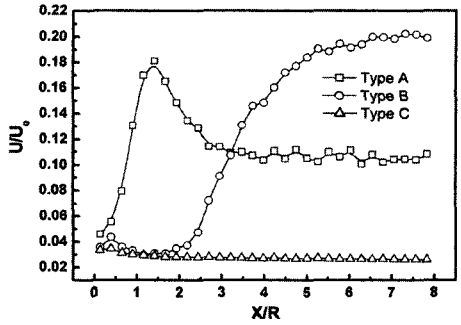

Fig. 3 Mean velocity U profiles along the centerline in the horizontal plane

Three burner models adopted in this study are considered as Type B with only slits, Type C with only swirl vanes, and Type A corresponding to main gas burner (Kim, 2003 ; Kim et al., 2003).

The measurement position of an X-probe in the X-Y plane (horizontal plane) along the downstream was selected at 10mm intervals from 5mm departed from a burner front for protecting a sensor to 305mm. On the other hand, as to the radial distance (Y), it was changed from −70mm to 70mm at 5mm intervals per position around the center of a burner model. Here, because the velocity ejected from the eight narrow slits situated radially on the edge of a burner model has the largest values, the velocity measurements near these narrow slits were carried out with traversing X-probe by 1mm in order to measure a flow velocity in detail.

The room temperature was controlled under the condition of about 19±0.5℃ for reducing the error due to temperature change.

3. Results and Discussion

3.1 Mean velocity profiles

Figure 3 shows the nondimensional profiles of axial mean velocity component normalized by the maximum exit velocity (U_e) for each burner model, where R is the draft tube radius of a burner. These values are equivalent to axial mean velocity components (U) for three burner models along the centerline in the X-Y plane.

In case of Type B with only slits, the axial mean velocity component along the centerline beyond

about X/R=1.5 increases remarkably because the jet flow, spouted from Y/R=±0.97 corresponding to narrow slits, spreads into the central part of the burner. However, in case of Type C with only swirl vanes, the rotational flow by swirl vanes was actually disappeared in axial direction because the axial mean velocity component is almost zero value except the initial region of the centerline. On the other hand, in case of Type A composed of slits and swirl vanes at the same time, the axial mean velocity component has not only the peak value of about 18% in the vicinity of X/R=1.5, but also the constant value of about 11% beyond about X/R=3.5. Thus, it can be known that while the slits and swirl vanes play a role increasing flow speed in the central part of a burner until about X/R=3.5, they also play a part reducing flow speed of Type B beyond about X/R=3.5.

Figure 4 shows the axial mean velocity profiles represented nondimensionally by the maximum exit velocity for each burner model. These values were also measured respectively for three burner models along the radial distance at four axial places in the horizontal plane.

All of the axial mean velocity components present a relatively symmetric distribution with respect to Y=0 regardless of the increase of axial distance. In case of Type C, because the rotational flow by swirl vanes spreads remarkably toward the radial direction at the position of X/R=0.1282, equivalent to the relatively initial flow region, the axial mean velocity component shows not only the peak value of about 40% larger than

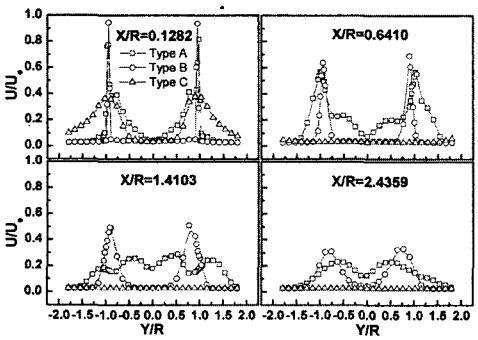

Fig. 4 Mean velocity U profiles along the radial direction in the horizontal plane

the maximum exit velocity around the outside radius of swirl vanes, but also a relatively larger velocity distribution in the outside of a burner. However, the axial mean velocity of Type A does not exist almost in the outer region unlike Type C. This is attributed to the fact that the fast jet spouted from slits encircles the rotational flow expanding radially toward the outer region by the swirl vanes. Therefore, the axial mean velocity component of Type A shows a similar magnitude distribution to that of Type B in the outer region as well as Type C in the central part of a burner. On the other hand, the axial mean velocity component of Type C appears changelessly with the magnitude, close to an almost zero value regardless of radial distance, as the axial distance increases. However, for the case of Type B, it shows a diffusing tendency toward the outer region as well as the central part although its peak value appearing in the vicinity of slits is reduced. Therefore, the peak value of Type A is smaller than that of Type B near the slits, but it shows a larger value in the central part.

Hibara et al. (1999) has pointed that if swirling flow jet strongly exists, the axial mean velocity component near the nozzle exit shows the peculiar velocity profile of swirling flow having the smallest value in the vicinity of central jet axis as well as the largest value in the outside. As the flow goes downstream, they conformed that the gradient of axial mean velocity profile in the central part decreases because the slow fluid speed in the central part accelerates and the fast fluid speed in the outside decelerates. Also, Gursul (1996) has described that the axial mean velocity component near the nozzle exit has a maximum value in the central jet axis in the case of nonswirling jet, but it shows a velocity profile just like a wake that is caved in the central jet axis in the case of swirling jet.

Figures 5 and 6 show the profiles of radial and tangential mean velocity components, normalized respectively by the maximum exit velocity for each burner model. These results were also measured with the same experimental method as shown in Figure 4.

In case of Type B, the radial mean velocity

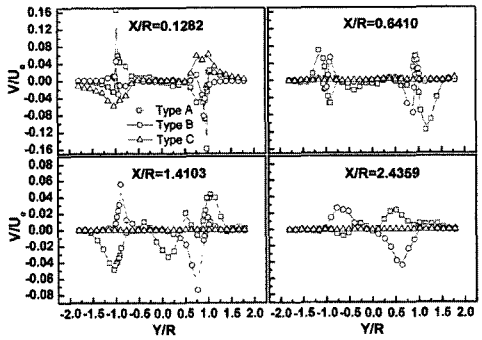

Fig. 5 Mean velocity V profiles along the radial direction in the horizontal plane

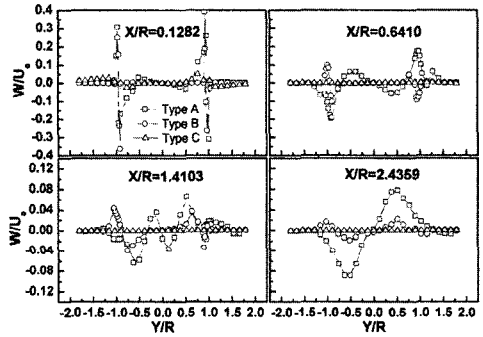

Fig. 6 Mean velocity W profiles along the radial direction in the horizontal plane

component (V) is largely formed in the vicinity of $Y/R=\pm0.97$ corresponding to slits, and its peak value is distributed with the different sign in the left and right radial position. In addition, its peak value decreases and develops to the central part as the axial distance increases. On the other hand, the tangential mean velocity component (W) shows a similar distribution, but its peak value is larger than that of V at all axial positions. In case of Type C, the radial mean velocity component and the tangential one are only formed around the outer region of swirl vanes at the position of $X/R=0.1282$, and their values have the same sign and a similar magnitude each other. The radial mean velocity component of Type A shows a quite different distribution from that of Type B and Type C. Especially, its peak value formed around the region of $Y/R=\pm0.97$ is larger than that of Type B and Type C. In addition, the radial mean velocity of Type A shows a comparatively symmetric distribution with respect to the center point until $X/R=1.4103$. The mean velocity V has a decreased peak value in absolute magnitude and develops to the central part due to the flow diffusion as the axial distance increases. The mean velocity W of Type A shows a similar development process as the axial distance increases although it has a different absolute magnitude around the region between slits and swirl vanes. Here, the mean velocity W of Type A is more largely distributed than that of V, and it shows more symmetric distribution with respect to the center point than V. It can be known that W depends on the rotational flow by swirl vanes more than V.

The extraordinary thing in Figs. 5 and 6 is that the mean velocities of V and W of Type A formed in the central part mix more actively than those of Type B and Type C due to the interaction between slit jet and swirling flow.

3.2 Turbulence intensity profiles

Figure 7 shows the turbulence intensity profiles of each directional component for three burner models along the centerline in the horizontal plane. These turbulence intensities (namely, u/U_e, v/U_e, w/U_e) were obtained by dividing RMS (Root-Mean-Square) values (namely, u, v, w) of axial, radial, and tangential fluctuation velocities respectively with the maximum exit velocity.

In case of Type B, the turbulence intensity components of each direction show the smallest value in the vicinity of $X/R=1.5$ and abruptly increase with the axial distance until about $X/R=3.5$. In addition, they show the largest value in the vicinity of $X/R=3.5$, but they are slowly reducing since $X/R=3.5$ even though the magnitude difference of them does not appear greatly. In case of Type C, the turbulence intensity components of each direction seem to be nearly disappeared in the whole range of axial distance except about $X/R<1.5$ because they are distributed with a very small value, almost equal to zero apparently, since about $X/R=1.5$. On the other hand, in case of Type A, the axial turbulence intensity component is distributed with the largest value. However, while the turbulence intensity component of Y-direction shows a larger

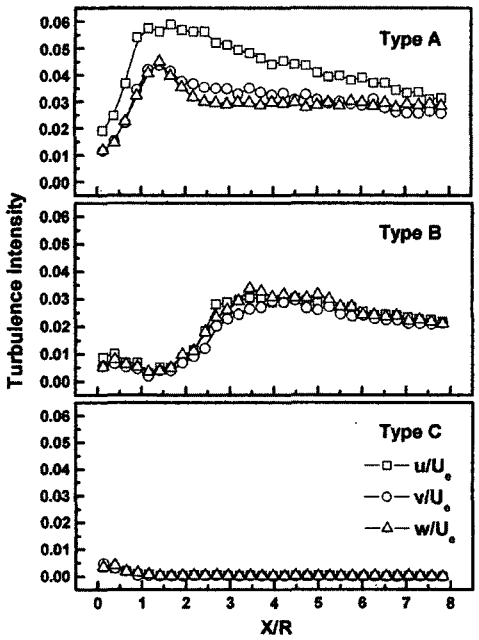

Fig. 7 Turbulence intensity profiles along the centerline in the horizontal plane

value than that of Z-direction in some regions, it is similar in magnitude to that of Z-direction as a whole. Specially, turbulence intensities of each directional component show their own maximum value in the vicinity of X/R=1.5 respectively because the turbulence mixing phenomenon of each direction acts the most greatly in the vicinity of X/R=1.5, and what is more, they keep decreasing gradually and a fixed magnitude beyond the position of X/R=1.5. Here, it can easily be known that these results are quite different phenomena from those of both Type B and Type C.

Figure 8 shows the turbulence intensity profiles of axial component for three burner models along the radial distance respectively at four axial places in the horizontal plane. These values were also calculated with the same method as shown in Fig. 7.

In case of X/R=0.1282 corresponding to the nearly initial region of a burner, the axial turbulence intensity component of Type B has a much smaller peak value than that of other two burner models because of undeveloped turbulence at Y/R=±0.97 equivalent to slits. Also it shows a very small value distribution along the all radial distance except Y/R=±0.97. Moreover, in case of Type C, the axial component of turbulence intensity shows a larger value distribution from the outside of swirl vanes, and also it presents a larger value distribution, compared with other two burner models at the outer location departed from slits. This can be regarded as a factor that the rotational flow by swirl vanes raises turbulence effectively in spite of nearly initial region of a burner. In case of X/R=0.6410, the axial turbulence intensity component of Type A accomplishes the largest value distribution among all models in whole radial area. However, in case of Type C, it shows an almost zero value at all radial positions except some outer region of a burner. On the other hand, for the region beyond X/R=1.4103, the axial turbulence intensity component of Type A is distributed with a comparatively larger value than that of other burner models, covering whole radial area with the central part, except some region near the slits.

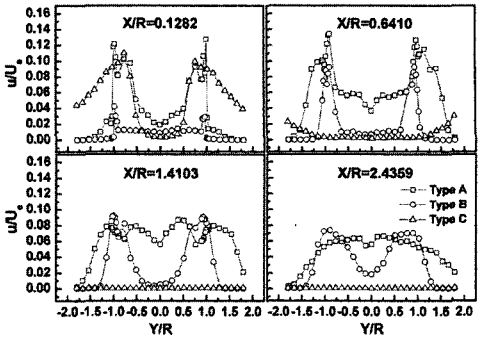

Fig. 8 Turbulence intensity u profiles along the radial direction in the horizontal plane

Figures 9 and 10 show the turbulence intensity profiles of radial and tangential components respectively for three burner models along the radial distance at four axial places in the horizontal plane. These values were also obtained with the same method as the axial turbulence intensity component was calculated.

Although the turbulence intensities of radial and tangential components respectively along the radial distance are some different from those of axial component in magnitude, they show a very similar distribution on the whole. Specially, in case of Type A, it can easily be known that the

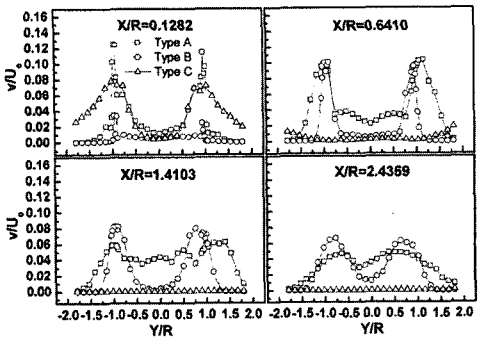

Fig. 9 Turbulence intensity v profiles along the radial direction in the horizontal plane

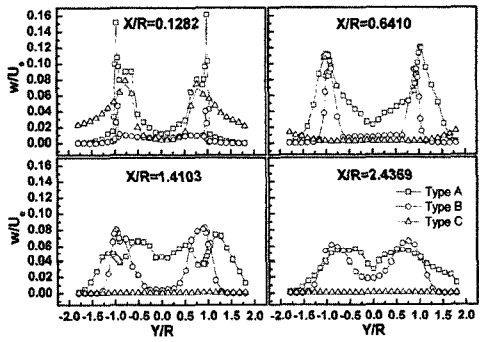

Fig. 10 Turbulence intensity w profiles along the radial direction in the horizontal plane

turbulence intensities of axial component shown in Fig. 8 is distributed with a little bit more larger value than those of radial and tangential components shown in Figs. 9 and 10 respectively according to the increase of axial distance. Consequently, it is evident that above facts are also in accord with the tendency of turbulence intensity profiles along the centerline. On the other hand, all turbulence intensity components along the radial distance still include two peaks near the slits at four axial places like Type B model. However, Type A shows no prominent peak beyond X/R=1.4103. This may result from the fact that the fast jet by slits encircles the rotational flow expanding radially toward the outer region by the swirl vanes and drives the mixed flow between slit jet and rotational flow toward axial downstream. Therefore, the slow rotational flow located in the boundary front interrupts the fast slit jet. As a result, the gradient of the mean velocity decreases along the radial

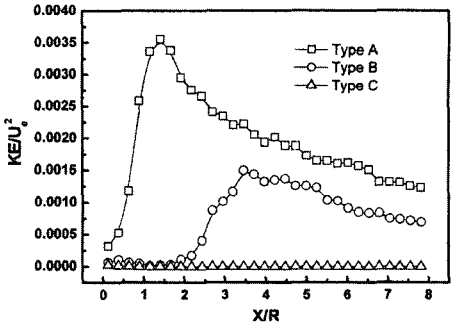

Fig. 11 Turbulent kinetic energy profiles along the centerline in the horizontal plane

distance, and then the turbulence intensity comparatively decreases a little beyond the position of X/R=1.4103. Therefore, the influence by slits decreases more and more. On the contrary, because the influence of rotational flow in the central part comparatively increases, the turbulence intensity increases due to an active turbulence mixing. On the whole, the turbulence intensity profile of Type A along the radial distance becomes more flat in the central part except the edge as the axial distance increases.

3.3 Turbulent kinetic energy profiles

Figure 11 shows the turbulent kinetic energy profiles for three burner models along the centerline in the horizontal plane. These values were obtained by dividing the turbulent kinetic energy $KE=(u^2+v^2+w^2)/2$ with the square of maximum exit velocity (U_e^2). Here, the square of RMS value of axial fluctuation velocity component involved in the above parenthesis, for example, means the variance of axial fluctuation velocity component.

The turbulent kinetic energies of Type A, which are formed along the centerline of the same axial position, were distributed with larger values than those of Type B or Type C, and it shows the largest value of about 0.35% in the vicinity of X/R=1.5. Moreover, it shows an up and down trend in front of and behind X/R=1.5. Here, the reason why the turbulent kinetic energy of Type A shows larger peak values than that of any other burner model in the centerline of about X/R=1.5 is attributed to the fact that both slits and swirl

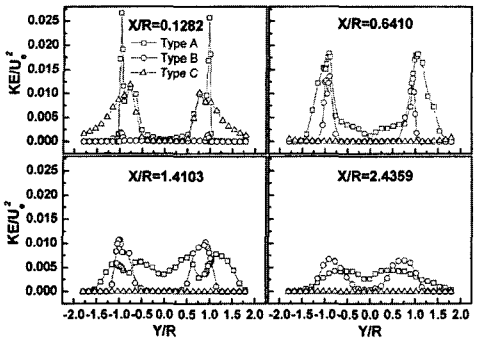

Fig. 12 Turbulent kinetic energy profiles along the radial direction in the horizontal plane

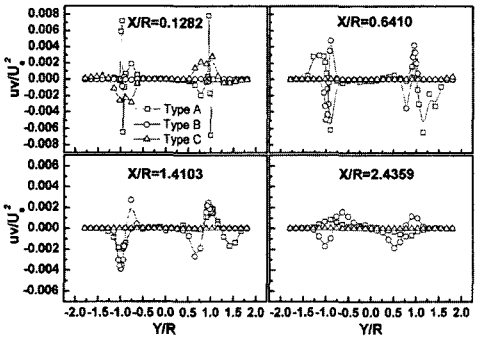

Fig. 13 Reynolds shear stress uv profiles along the radial direction in the horizontal plane

vanes increase turbulence level largely in the initial region, compared with other models in consequence of their flow control due to their coexistence in this region.

Figure 12 shows the turbulent kinetic energy profiles obtained respectively for three burner models along the radial distance at four axial places in the horizontal plane. These values were also obtained with the same method as the nondimensional turbulent kinetic energies shown in Fig. 11 are calculated.

The turbulent kinetic energy of Type A shows not only the largest value of about 2.7% near the slits at the position of X/R=0.1282, but also the same magnitude distribution as that of Type C because of rotational flow by swirl vanes located in the inner part of a baffle plate. Moreover, the turbulent kinetic energy of Type B hardly exists at all radial positions except that it only shows a very small value near the slits. Especially, the turbulent kinetic energy of Type C does not exist regardless of the increase of axial distance except near the slits at the position of X/R=0.1282. On the other hand, in case of Type A, while the peak values of turbulent kinetic energy near the slits decrease with axial distance, they increase relatively in the central part. Also, in case of Type B, the peak values near the slits beyond X/R=1.4103 is distributed with a much larger magnitude than that of Type A because the effect of swirl vanes is excluded.

3.4 Reynolds shear stress profiles

Figures 13 and 14 show the Reynolds shear stress profiles normalized by the square of maximum exit velocity for each burner model at four axial positions in the horizontal plane.

The Reynolds shear stresses uv and uw of Type B have very small values due to undeveloped turbulence intensity even around the region of Y/R=±0.97, equivalent to slits at the initial location of X/R=0.1282. However, the Reynolds shear stress uv shows a remarkably increased peak value around the region of slits at the position of X/R=0.6410. Moreover, as the axial distance increases, its peak value shows a gradually decreasing tendency and shifts itself toward the central part. Here, compared with the Reynolds shear stress uw of Type B, the uv distribution shows a little larger value near the slits and in the central part at all axial positions. In case of Type C, the Reynolds shear stress uv as well as uw have large values, nearly same magnitude and pattern around the region of swirl vanes only at the initial location of X/R=0.1282. On the other hand, for the case of Type A, the Reynolds shear stresses uv and uw show a quite different distribution, compared with those of Type B and Type C This seems to be caused by the interaction between slit jet and rotational flow by swirl vanes, developing turbulence intensity effectively. Especially, the Reynolds shear stresses uv and uw formed at the initial position of X/R=0.1282 for Type A show large positive and negative peak values near the slits due to the gradient of radial and tangential mean velocity component, respectively. In addition, they have a second peak value around the outer region of swirl vanes.

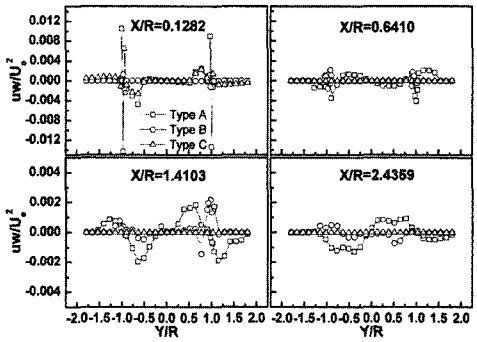

Fig. 14 Reynolds shear stress uw profiles along the radial direction in the horizontal plane

As a whole, because the Reynolds shear stresses uv and uw develop and diffuse to the central part as the axial distance increases, their peak values decrease in the region near the slits, but increase in the central part. Therefore, they show a very small value having a gentle slope difficult to discriminate the magnitude difference on the whole range beyond the location of X/R=2.4359, compared with the magnitude of initial region. On the other hand, the Reynolds shear stress uw for Type A in the central part until X/R=0.6410 exists more largely than uv in magnitude and slope. It may be thought that this is attributed to the fact that the tangential turbulent velocity component acts more largely in these regions due to swirling flow by swirl vanes.

Kihm et al. (1990) found that the Reynolds shear stress has a negative and positive value according to the positive and negative gradients of the mean velocity profiles. For swirling flows, the turbulent shear stress distribution is strongly anisotropic (Lilley et al., 1971).

4. Conclusions

The gun-type gas burner adopted in this study is generally designed as the arrangement of eight slits, eight swirl vanes, and a cone-type baffle plate, etc. Thus, in order to analyze the effects of slits and swirl vanes on the turbulence augmentation in a main burner, axial mean velocity component and turbulent characteristic values were measured by using an X-type hot-wire probe for three burner models. The results can be summarized as follows.

(1) As the axial distance increases, the axial mean velocity component of Type A decreases near the slits, but it increases in the central part of a burner. Especially, both slits and swirl vanes increase an axial mean velocity component in the central part more highly than that of Type B until $X/R \leq 3.5$, and vice versa beyond the location of $X/R > 3.5$. Consequently, the axial mean velocity component of Type A along the centerline shows not only a peak value of about 18% larger than the maximum exit velocity at about X/R=1.5, but also a comparatively constant value of about 11% beyond about X/R=3.5.

(2) All turbulence intensities measured for Type A have not only larger values than those of Type B or Type C in the central part of a burner, but also a peak value at about X/R=1.5. Therefore, the slits and swirl vanes can be regarded as a useful tool to increase turbulence intensities remarkably in a gun-type gas burner.

(3) The turbulent kinetic energy of Type A is distributed with a fairly larger value than that of Type B or Type C near the slits in spite of comparatively initial region until $X/R \leq 0.6410$ because rotational flow by swirl vanes and fast jet flow by slits coexist in order to increase turbulence intensities effectively, and it shows a much larger value than any other burner model in the central part beyond X/R=0.6410.

(4) The Reynolds shear stresses uv and uw of Type A show a quite different magnitude and distribution from those of Type B and Type C because the interaction between slit jet and rotational flow by swirl vanes develops the turbulence intensity effectively. They show a large positive and negative peak value near the slits in spite of the initial region of X/R=0.1282. On the other hand, the Reynolds shear stress uw of Type A in the central part until X/R=0.6410 exists more largely than uv in magnitude and slope.

Acknowledgment

This work was partially supported by the Fisheries Science Institute of Kunsan National University in 2003.

References

Beer, J. M. and Chigier, N. A., 1972, *Combustion Aerodynamics*, John Wiley & Sons Press, New York, pp. 102~104.

Bruun, H. H., 1996, *Hot-Wire Anemometry*, Oxford Science Publications, pp. 132~163.

Chen, R. H. and Driscoll, J. F., 1988, "The Role of Recirculation Vortex in Improving Fuel-Air Mixing Within Swirling Flames," *22nd Symp. (International) on Combustion*, The Combustion Institute, Pittsburgh, PA, pp. 531~540.

Dantec, 2000, *Streamline User's Reference Manual*, Chapter 8.3 Algorithms.

Froud, D., O'doherty, T. and Syred, N., 1995, "Phase Averaging of the Precessing Vortex Core in a Swirl Burner under Piloted and Premixed Combustion Conditions," *Combustion and Flame*, Vol. 100, pp. 407~412.

Gupta, A. K., Beer, J. M. and Swithenbank, J., 1976, "Concentric Multi-Annular Swirl Burners: Stability Limits and Emission Characteristics," *16th Symp. (International) on Combustion*, The Combustion Institute, Pittsburgh, PA, pp. 79~91.

Gupta, A. K., Lilley, D. G. and Syred, N., 1984, *Swirl Flows*, Abacus Press, Tunbridge, England.

Gursul, I., 1996, "Effect of Nonaxisymmetric Forcing on a Swirling Jet With Vortex Breakdown," *Trans. ASME, J. of Fluids Eng.*, Vol. 118, pp. 316~323.

Hibara, H. and Sudou, K., 1999, "Swirling Jet along a Solid Surface," *Trans. JSME (Part B)*, Vol. 65, No. 629, pp. 130~137 (In Japanese).

Kihm, K. D., Chigier, N., and Sun, F., 1990, "Laser Doppler Velocimetry Investigation of Swirler Flowfields," *J. Propulsion*, Vol. 6, No. 4, pp. 364~374.

Kim, J. K., 2001, "Investigation of the Three-Dimensional Turbulent Flow Fields of the Gas Swirl Burner with a Cone Type Baffle Plate (I)," *KSME Int. J.*, Vol. 15, No. 7, pp. 895~905.

Kim, J. K., 2001, "Investigation of the Three-Dimensional Turbulent Flow Fields of the Gas Swirl Burner with a Cone Type Baffle Plate (II)," *KSME Int. J.*, Vol. 15, No. 7, pp. 906~920.

Kim, J. K., 2001, "An Experimental Study on Three Dimensional Turbulent Flow Characteristics of Swirl Burner for Gas Furnace," *Trans. KSME (Part B)*, Vol. 25, No. 2, pp. 225~234 (In Korean).

Kim, J. K. and Jeong, K. J., 2003, "The Role of Slits and Swirl Vanes on the Turbulent Flow Fields in Gun-Type Gas Burner with a Cone-Type Baffle Plate," *Trans. KSME (Part B)*, Vol. 27, No. 4, pp. 466~475 (In Korean).

Kim, J. K., 2003, "The Effect of Slits and Swirl Vanes on the Development of Turbulent Flow Fields in Gun-Type Gas Burner," *Trans. KSME (Part B)*, Vol. 27, No. 9, pp. 1299~1308 (In Korean).

Kim, J. K. and Jeong, K. J., 2004, "Investigation on the Turbulent Flow Characteristics of a Gun-Type Gas Burner with the Different Shape of Baffle Plate," *Trans. KSME (Part B)*, Vol. 28, No. 4, pp. 475~485 (In Korean).

Lefebvre, A. H., 1983, *Gas Turbine Combustion*, pp. 126~135.

Leuckel, I. W. and Fricker, N., 1976, "The Characteristics of Swirl-Stabilized Natural Gas Flames," *J. Inst. Fuel*, Vol. 49, pp. 103.

Lilley, D. G. and Chigier, N. A., 1971, "Nonisotropic Turbulent Shear Stress Distribution in Swirling Flows from Mean Value Distributions," *Int. J. of Heat and Mass Transfer*, Vol. 14, pp. 573~585.

Shioji, M., Kim, I. S., Ikegami, M., and Murakami, K., 1998, "Flame Stability and NOx Formation in a High-Intensity Swirl Burner," *Trans. JSME (Part B)*, Vol. 64, No. 621, pp. 222~227 (In Japanese).

Syred, N. and Beer, J. M., 1974, "Combustion in Swirling Flows: A Review," *Combustion and Flame*, Vol. 23, pp. 143~201.

Tsao, J. M. and Lin, C. A., 1999, "Reynolds Stress Modeling of Jet and Swirl Interaction Inside a Gas Turbine Combustor," *Int. J. for Numerical Methods in Fluids*, Vol. 29, pp. 451~464.